

PCCP

Accepted Manuscript



This is an *Accepted Manuscript*, which has been through the Royal Society of Chemistry peer review process and has been accepted for publication.

Accepted Manuscripts are published online shortly after acceptance, before technical editing, formatting and proof reading. Using this free service, authors can make their results available to the community, in citable form, before we publish the edited article. We will replace this *Accepted Manuscript* with the edited and formatted *Advance Article* as soon as it is available.

You can find more information about *Accepted Manuscripts* in the [Information for Authors](#).

Please note that technical editing may introduce minor changes to the text and/or graphics, which may alter content. The journal's standard [Terms & Conditions](#) and the [Ethical guidelines](#) still apply. In no event shall the Royal Society of Chemistry be held responsible for any errors or omissions in this *Accepted Manuscript* or any consequences arising from the use of any information it contains.

Tensile Strain Induced Half-Metallicity in Graphene-like Carbon Nitride

Hengshuai Li^{a,b}, Haiquan Hu^c, Chunjiang Bao^b, Juan Hua^a, Hongcai Zhou^a,
Xiaobiao Liu^a, Xiangdong Liu^a, Mingwen Zhao^{a,*}

Abstract

Polymeric graphitic carbon nitride materials exhibit exotic properties superior to graphene which are promising for applications in energy conversion, environment protection, and spintronics devices. We propose a two-dimensional (2D) framework of graphene-like carbon nitride composing of C_9N_7 units connected by nitrogen atoms. From first-principles, we demonstrate that this 2D carbon nitride has a spin-polarized ground state and exhibits metallic electronic properties, in contrast to commonly studied graphitic carbon nitrides which are nonmagnetic semiconductors. Additionally, half-metallicity can be achieved in this framework by applying tensile strain. The realization will be beneficial for spintronics as a candidate material for a spin-current generator. More importantly, this provides a feasible way to realize half-metallicity in experiments.

^a*School of Physics and State Key Laboratory of Crystal Materials, Shandong University, Jinan 250100, China. E-mail: mingwen.zhao@gmail.com*

^b*School of Mechanical & Automotive Engineering, Liaocheng University, Liaocheng, 252059, China*

^c*School of Physics Science and Information Technology, Liaocheng University, Liaocheng, 252059, China*

1. Introduction

The intriguing physical properties of graphene, a two-dimensional (2D) aromatic monolayer of carbon atoms, triggered keen interest in 2D nanosheets other than carbons. Although some of them have been demonstrated to have many exceptional properties, this field is still in its infancy when compared to graphene. An interesting example is graphitic carbon nitrides whose history can be traced back to more than one hundred years ago.¹⁻³ Recently, interests in polymeric graphitic carbon nitrides were aroused owing to its potential applications in energy conversion, environment protection, and spintronic devices. Up to now, graphitic carbon nitrides can be synthesized through different approaches.⁴⁻¹² There are two prevailing models of the graphitic carbon nitrides. One has triazine (C_3N_3) as building blocks (referred to as s-triazine), while the building blocks of another model, tri-s-triazine (heptazine) rings, resemble the hypothetical polymer melon.¹³⁻¹⁸ These building blocks are cross-linked by triangular nitrogen atoms (joint N), forming 2D defect-rich and nitrogen-bridged honeycomb lattices (g- C_3N_4). Theoretical studies have shown that the latter model is energetically more favorable than the former one.^{17,18} These g- C_3N_4 materials are semiconductors with band gaps of 1.16 eV and 0.89 eV, respectively.¹⁹ This makes the g- C_3N_4 function as a metal-free polymeric photocatalyst for splitting water molecules with solar energy.²⁰

Inducing stable electron spin-polarization and even half-metallicity in graphitic carbon nitrides is an urgent demand for spintronics which seeks to exploit the electron spin in addition to the electrical charge for logic and memory devices. A key challenge in this area is the generation of 100% spin-polarized currents at the Fermi level. Half-metals which can filter the current into a single spin channel fully meet this demand.^{21,22} Up to now, a large number of materials, such as manganese perovskites,²³ Heusler compounds,²⁴ the metal-DNA complex,²⁵ the transition metal doped dilute magnetic semiconductor,²⁶ and silicon nanowire and heterostructures^{27,28} have been proved to be half-metals, where transition metals (TMs) are believed to be responsible for the half-metallicity. However, TM-contained systems may not be

compatible with many current matured technologies based on main group semiconductors. Additionally, the strong coupling between spins of carriers and the TMs will result in a very short spin relaxation time, greatly impacting on the performance of spintronics devices.

Therefore, some new strategies have been proposed to realize TM-free half-metallicity.^{29–42} For examples, Kan et al. predicted half-metallicity in an edge modified zigzag graphene nanoribbon by a small organic molecule or B/N dopants.^{29–32} The experimental challenging of these strategies lies in the fine control positions of functional groups or the B/N dopant. Hydrogenations of graphene or an h-BN sheet have also been reported to induce ferromagnetism and half-metallicity.^{33,34} However, the experimental realization of hydrogenation remains a big challenge by the current technologies because they are often formed in a random way on a host structure. All the theoretically predicted half-metallicity in C/BN-based compounds needs either the carefully selective doping^{29–32} or a strong external electric field,^{38,43,44} which may make the experimental synthesis largely inaccessible.

In a recent work of Du et al, they demonstrated from first-principles that stable half-metallicity can be achieved in a new type of graphitic carbon nitride (g-C₄N₃) whose structure can be characterized by substituting the joint nitrogen atoms with carbon atoms in the framework of s-triazine-based g-C₃N₄.⁴⁵ This opens a door for seeking TM-free half-metals, because graphitic carbon nitride may have abundant polytypes.

In this work, we propose another 2D framework of carbon nitride using C₉N₇ units as building blocks. These units are connected by nitrogen atoms resulting in a graphene-like carbon nitride with a stoichiometry of C₉N₇ (referred to as g-C₉N₇). From first-principles, we demonstrate that this g-C₉N₇ has a spin-polarized ground state, similar to the case of g-C₄N₃. More interestingly, the spin polarization of carriers near the Fermi level can be tuned by applying tensile strain. Half-metallicity can be achieved under certain tensile strain. The realization will be beneficial for spintronics as a candidate material for a spin-current generator or a strain sensor.

2. Method and computational details

Our first-principles calculations were performed within the framework of density-functional theory (DFT), which is implemented in the Vienna ab initio simulation package known as VASP.⁴⁶⁻⁴⁸ The electron-electron interactions were treated using a generalized gradient approximation (GGA) in form of Perdew-Burke-Ernzerhof (PBE) for the exchange-correlation functional.⁴⁹ The energy cutoff employed for plane-wave expansion of electron wavefunctions was set to 500eV. The electron-ion interactions were described by projector-augmented-wave (PAW) potentials.^{50,51} Four electrons for carbon ($2s^22p^2$) and five electrons for nitrogen ($2s^22p^3$) were treated as valence electrons. The supercells were repeated periodically on the x-y plane while a vacuum region of 15 Å was applied along the z-direction to avoid mirror interactions between neighboring images. The BZ integration was sampled on a grid of $15 \times 15 \times 1$ k-points. Structural optimizations were carried out using a conjugate gradient (CG) method until the remaining force on each atom was less than 0.001 eV/Å.

3. Results and discussion

The structure of the g-C₉N₇ has a center benzene ring surrounded by three CN pentagons, as shown in Figure 1(a). These g-C₉N₇ building blocks are then joined together by nitrogen atoms through C-N bonds, forming a two-dimensional honeycomb lattice with a chemical formula of C₉N₇ per primitive cell. Structural optimization indicates that the energetically most preferable structure has planar configuration with six-fold symmetry. The energy difference between planar and buckled configurations with a height of 0.08 Å is below 0.5 meV/cell, which implies the high flexibility. The lengths of the two C-N bonds in the pentagons are 1.33 Å and 1.37 Å, respectively, both of which are slightly longer than that in g-C₃N₄ (1.327 Å). The C-N bonds that connect the s-triazines are 1.42 Å in length, longer than that in g-C₄N₃ (1.347Å). The relevant structural parameters are listed in Table 1.

Table 1

Structural parameters and formation energies (E_{form}) of two-dimensional carbon nitride lattices: Bond length of C-N bonds ($d_{\text{C-N}}$), bond angle between two C-N bonds ($\angle\text{C-N-C}$) in s-triazine ring, lattice constant (a) and formation energy (E_{form}).

Lattices	$d_{\text{C-N}}(\text{\AA})$	$\angle\text{C-N-C}(\text{\textcircled{C}})$	a (A)	$E_{\text{form}}(\text{eV/atom})$	
				N-rich	C-rich
g-C ₃ N ₄	1.327	116.1	4.785	0	0
g-C ₄ N ₃	1.349	120.9	4.833	-0.006	0.194
g-C ₉ N ₇	1.33 1.37	120	8.05	-1.504	-0.764

Similar structures have been synthesized in the experiment,⁵²⁻⁵⁶ convincing the plausibility of this g-C₉N₇ framework. We also evaluated the energetic stability with respect to the already-synthesized g-C₃N₄.¹⁷ We defined the formation energy (E_{form}) of the graphene-like carbon nitride (g-C_xN_y) as follow.

$$E_{\text{form}} = E_{\text{g-C}_x\text{N}_y} - x \times \mu_{\text{C}} - y \times \mu_{\text{N}}$$

$E_{\text{g-C}_x\text{N}_y}$ is the total energy of g-C_xN_y, μ_{C} and μ_{N} are the chemical potentials of C and N atoms which are highly dependent on specifically employed atomic reservoirs. Here, we considered two limits: nitrogen-rich (N-rich) and carbon-rich (C-rich) environment. In N-rich medium, μ_{N} was calculated from nitrogen molecule in gas phase, while under C-rich condition, μ_{C} was calculated from graphene monolayer. In both cases, the chemical potentials of the two atoms are jointed together via the restriction: $3 \times \mu_{\text{C}} + 4 \times \mu_{\text{N}} = E_{\text{C}_3\text{N}_4}$, where $E_{\text{C}_3\text{N}_4}$ is the total energy per C₃N₄ unit in g-C₃N₄. Our calculations show that the g-C₉N₇ framework is energetically more favorable than the already-synthesized g-C₃N₄ by -0.764 eV/atom (C-rich) and -1.504 eV/atom (N-rich) in both conditions. Additionally, we performed molecular dynamics (MD) simulations to test the dynamic stability of g-C₉N₇. A large (3×3) supercell containing 144 atoms is simulated with a Nose-Hoover thermostat at 300 K. After 30 ps, we didn't find any structure destruction, which implies the stability of the g-C₉N₇ at room temperature. The kinetic stability of the framework was also checked from the phonon spectrum obtained by using the force-constant theory combined with the VASP code. The phonon dispersion relations along high-symmetric directions in BZ

were plotted in Figure 1(b). Clearly, the phonon spectrum is free from imaginary frequencies, suggesting that the g-C₉N₇ framework is kinetically stable. The optical and acoustical branches are well separated in the spectrum. Two acoustical branches have linear dispersion relations near the center of BZ (Γ point). It is noteworthy that the transverse acoustical phonon branch has no imaginary frequencies near the Γ point in contrast with the cases of germanium silicide⁵⁷ and siligraphenes⁵⁸. This suggests that the g-C₉N₇ framework is stable for the particular mode with long wavelength.

Because X-ray diffraction (XRD) spectra are quite useful for characterization of novel synthesized materials, we simulated the XRD spectrum of the g-C₉N₇ framework with a wavelength of 1.540562 Å. The XRD spectra of the already-synthesized g-C₃N₄ and g-C₄N₃ lattices were also presented for the purpose of comparison.⁵⁹ It is clear that these three materials have sharp peaks at $2\theta=8.84^\circ$ and 17.72° , corresponding to their (002) and (004) planes as showed in Figure1(c). However, g-C₉N₇ has additional peaks at $2\theta=11.3^\circ$, and 14.4° , which can be regarded as finger prints to identify the g-C₉N₇ from other graphitic carbon nitride materials.

The electronic structures of the g-C₉N₇ are then studied. It is interesting to see that g-C₉N₇ has a spin-polarized ground state with a magnetic moment of $0.6\mu_B$ in per unit cell. From Figure 2(a), two energy bands cross the Fermi level, leading to nonzero electron density of states (DOS) at the Fermi level, implying the metallic properties of the g-C₉N₇. This differs completely from the semiconducting properties of g-C₃N₄. The spatial distribution of the spin-polarized electron density, as shown in Figure 2(b) suggests that the metallic properties are closely related to the p_z atomic orbitals in the framework. This feature is more obvious from the electron density of states (PDOS) projected onto different atoms (C1, C2, N3, and N4), as shown in Figure 2(c) and Figure 3. The electron states near the Fermi level arise mainly from the p_z orbitals of C1, C2, and N4 atoms. The C2 atom has been well separated by nitrogen atoms (N3 and N4) which prevents the single p_z electron of C2 to form pair.^{60,61} The appearance of flat bands near the Fermi level is thus reasonable. However, from the PDOS, it is obvious that the C1 atoms also contribute to the flat bands. This is the reason why the spatial distribution of spin-polarized electron

density exhibits rather dispersive features, as shown in Figure 2(b). Although the p_z electrons of C2 atoms prefer to form π -bond in the hexagonal rings as the case of graphene, they are separated by the nitrogen atoms, which prevents the formation of conjugated π -orbitals throughout the framework. Moreover, nitrogen atom has one more electrons than carbon atom. The energy of the Fermi level is thus increased compared to the pristine carbon counterpart,⁶² giving rise to the metallic properties of the g-C₉N₇. The electron spin-polarization in the g-C₉N₇ can be attributed to the instability of electron in the partially-occupied flat bands, which leads to spin splitting to reduce the energy of system.

We also checked the spin-polarized ground state of the g-C₉N₇ lattice using a more accurate hybrid functional (HSE 06). It is found that electron band structures obtained from the hybrid functional remain spin-polarized, as shown in Figure 2(d), suggesting that the spin-polarized characteristics of the g-C₉N₇ framework are independent of the adopted exchange-correlation functional. The electronic band properties of the buckled g-C₉N₇ lattice were also calculated. The band structures of the planar and buckled configuration are very similar, including the electron spin-polarization characteristics. Structural buckling has less effect on the electronic properties of the g-C₉N₇ framework.

Considering the bands touching at the Γ point, it would be interesting to see if spin-orbital coupling (SOC) can open a gap at the touching point. Our first-principles calculations involving SOC indicated that the gap opened due to SOC is only 0.2 meV. This is related to the weak SOC of the p_z orbitals in the framework which is in fact a second order process.⁶³⁻⁶⁵

In order to study the possible reconstruction and magnetic coupling between local magnetic moments, we adopted large-size supercells containing four primitive cells (denoted as 2×2). Our self-consistent calculations start from different initial spin arrangements. One has the local magnetic moments aligned in a ferromagnetic way (FM) [Figure 4(a)], similar to the results of the primitive cells. The other one has the local magnetic moments aligned in an “antiferromagnetic” way (AFM) [Figure 4(b)]. The third one is nonmagnetic configuration (NM) [Figure 4(c)]. After

self-consistent calculations, we found both the AFM and NM configurations convert to a NM state which is energetically less stable than the FM state by about 33.11 meV. We didn't obtain the AFM state. This confirms the stability of the FM ordering in this framework. Additionally, the planar structure of the g-C₉N₇ is well preserved in the 2 × 2 supercell for both FM and NM states.

Finally, we investigate the stability of the ferromagnetic ordering under biaxial tensile strain. We mimic biaxial strain effects by expanding both in-plane lattice vectors. The energy difference between the FM and NM states, $\Delta E = E_{\text{FM}} - E_{\text{NM}}$, of the 2 × 2 supercell was used to evaluate the stability of the ferromagnetic ordering. The lower the ΔE value the more stable the FM ordering will be. The variation of ΔE as a function of tensile strain is shown in Figure 5(a). It is clear that the stability of FM ordering increases with the increase of tensile strain. The magnetic moment of the system is also shown in Figure 5(a). Along with the increase of tensile strain, the magnetic moment becomes larger. It is noteworthy that as the tensile strain exceeds 7%, there is a sudden drop in energy [Figure 5(b)], suggesting that the framework is fractured.

The evolution of the electron band structures in response to the tensile strain is quite interesting.⁶⁶ At a tensile strain of 2%, the band structure of g-C₉N₇ keeps the features of spin-polarized metals with two bands of spin-up and spin-down channels across the Fermi level, as shown in Figure 6(a). Compared with the equilibrium state, the splitting of the two spin channels is increased. At the tensile strain of 3% and 4%, the spin-up channel remains metallic, but the spin-down channel becomes semiconducting, as shown in Figure 6(b) and 6(c), leading to the transition from spin-polarized metal to half-metal. In order to determine the crucial tensile strain of the phase transition, we calculated the band gap (Δ) between the two spin channels defined in the Figure 6(d) at different tensile strain. $\Delta < 0$ and $\Delta > 0$ correspond to the spin-polarized metallic state and half-metallic state, respectively. $\Delta = 0$ gives the critical point of the phase transition. From Figure 6(d), the tensile strain at the critical point is about 2.4%. From the evolution of band structures, it can be found that the phase translation from spin-polarized metal to half-metal is mainly attributed to the

band near Fermi level. We therefore plotted the charge density of the flat band at the Γ (0,0,0) and K (2/3,1/3,0) points with and without tensile strain in Figure 7. It is obvious that the overlap of the wavefunctions decrease as the tensile is applied, leading to the localization of the electron states. The width of the flat bands decreased consequently. The localized electron states and narrow flat bands are advantageous for the electron spin polarization and lead to the appearance of half-metallicity. Similar mechanism has also been proposed for silicon nanosheets.⁶⁷ The achievement of tunable half-metallicity in this g-C₉N₇ framework is quite promising for application in spintronics devices, e.g. generating 100% spin-polarized current. More importantly, this provides a better way to realize half-metallicity, and this way is feasible in the experimental operation.

4. Conclusions

In summary, based on first-principles calculations, we propose a stable two-dimensional graphene-like carbon nitride material composing of C₉N₇ units, which has superior stability and own XRD spectrum. It possesses a ferromagnetic ground state and intrinsic metallicity, in contrast to commonly studied graphitic carbon nitrides which are nonmagnetic semiconductors. The stability of the ferromagnetic ordering can be improved by applying tensile strain. As the tensile strain exceeds 2.4%, the carbon nitride framework converts to a half-metal with 100% electron spin-polarization at the Fermi level. Such strain-induced half-metallicity in this metal-free framework may find application in spintronics devices.

Acknowledgements

This work is supported by the National Basic Research Program of China (No.2012CB932302), the National Natural Science Foundation of China (No.91221101), the 111 project (No.B13209), and National Super Computing Centre in Jinan.

References

- 1 J. V. Liebig, *Ann. Pharm.*, 1834, **10**, 10.
- 2 E. C. Franklin, *J. Am. Chem. Soc.*, 1922, **44**, 486 – 509.
- 3 L. Pauling, J. H. Sturdivant, *Proc. Natl. Acad. Sci. USA*, 1937, **23**, 615 – 620.
- 4 X. J. Bai, C. B. Cao, X. Y. Xu, *Mater. Sci. Eng. B*, 2010, **175**, 95–99.
- 5 G. F. Jiang, C. H. Zhou, X. Xia, F. Q. Yang, D. S. Tong, W. H. Yu, S. M. Liu, *Mater. Lett.*, 2010, **64**, 2718 – 2721.
- 6 B. Jürgens, E. Irran, J. Senker, P. Kroll, H. Müller, W. Schnick, *J. Am. Chem. Soc.*, 2003, **125**, 10208 – 10300.
- 7 L. Seyfarth, J. Seyfarth, B. V. Lotsch, W. Schnick, J. Senker, *Phys. Chem. Chem. Phys.*, 2010, **12**, 2227 – 2237.
- 8 A. V. Semench, L. N. Blinov, *Glass Phys. Chem.*, 2010, **36**, 199 –208.
- 9 Y. Wang, X. Chen Wang and M. Antonietti, *Angew. Chem. Int. Ed.*, 2012, **51**, 68.
- 10 R. C. Dante, P. Martín-Ramos, A. Correa-Guimaraes and J. Martín-Gil, *Mater. Chem. Phys.*, 2011, **130**, 1094.
- 11 F. Dong, L. Wu, Y. Sun, M. Fu, Z. Wu and S. C. Lee, *J. Mater. Chem.*, 2011, **21**, 15171.
- 12 M. Groenewolt and M. Antonietti, *Adv. Mater.*, 2005, **17**, 1789.
- 13 D. M. Teter and R. J. Hemley, *Science*, 1996, **271**, 53.
- 14 A. Y. Liu and R. M. Wentzcovitch, *Phys. Rev. B: Condens. Matter Mater. Phys.*, 1994, **50**, 10362.
- 15 J. Ortega and O. F. Sankey, *Phys. Rev. B: Condens. Matter Mater. Phys.*, 1995, **51**, 2624.
- 16 B. Jürgens, E. Irran, J. Senker, P. Kroll, H. Müller and W. Schnick, *J. Am. Chem. Soc.*, 2003, **125**, 10208.
- 17 E. Kroke, M. Schwarz, E. Horath-Bordon, P. Kroll, B. Noll and A. D. Norman, *New J. Chem.*, 2002, **26**, 508.
- 18 J. Sehnert, K. Baerwinkel and J. Senker, *J. Phys. Chem. B*, 2007, **111**, 10671.

- 19 Y. Xu and S. -P. Gao, *Int. J. Hydrogen Energ.*, 2012, **37**, 11072-11080.
- 20 X. Wang, K. Maeda, A. Thomas, K. Takanabe, G. Xin, J. M. Carlsson, et al., *Nat. Mater.*, 2009, **8**, 76.
- 21 D. D. Awschalom and M. E. Flatt, *Nature Phys.*, 2007,**3**, 153.
- 22 C. Felser, G. H. Fecher, and B. Balke, *Angew. Chem. Int. Ed.*, 2007, **46**, 668.
- 23 J. -H. Park, E. Vescovo, H. -J. Kim, C. Kwon, R. Ramesh, and T. Venkatesan, *Nature (London)*, 1998, **392**, 794.
- 24 R. A. de Groot, F. M. Mueller, P. G. vanEngen, and K. H. J. Buschow, *Phys. Rev. Lett.*,1983, **50**, 2024.
- 25 S. S. Mallajosyula and S. K. Pati, *J. Phys. Chem. B*, 2007, **111**,13877 .
- 26 J. E. Medvedeva, A. J. Freeman, X.Y. Cui, C. Stampfl, and N. Newman, *Phys. Rev. Lett.*, 2005, **94**, 146602.
- 27 H. Wu, P. Kratzer, and M. Scheffler, *Phys. Rev. Lett.*, 2007, **98**, 117202.
- 28 E. Durgun, D. Cakir, N. Akman, and S. Ciraci, *Phys. Rev. Lett.*, 2007, **99**, 256806.
- 29 E. Kan, Z. Li, J. Yang, and J. G. Hou, *J. Am. Chem. Soc.*, 2008, **130**, 4224.
- 30 S. Dutta, A. K. Manna, and S. K. Pati, *Phys. Rev. Lett.*, 2009, **102**, 096601.
- 31 S. Dutta and S. K. Pati, *J. Phys. Chem. B*, 2008, **112**, 1333.
- 32 Y. F. Li, Z. Zhou, P. W. Shen, and Z. F. Chen, *ACS Nano*, 2009, **3**, 1952.
- 33 J. Zhou, Q. Wang, Q. Sun, X. S. Chen, Y. Kawazoe, and P. Jena, *Nano. Lett.*, 2009, **9**, 3867.
- 34 W. Chen, Y. Li, G. Yu, C.-Z. Li, S. B. Zhang, Z. Zhou, and Z. Chen, *J. Am. Chem. Soc.*, 2010, **132**, 1699.
- 35 Y. L. Lee, S. Kim, C. Park, J. Ihm, and Y. W. Son, *ACS Nano*, 2010, **4**, 1345.
- 36 A. J. Du, Y. Chen, Z. H. Zhu, G. Q. Lu, and S. C. Smith, *J. Am. Chem. Soc.*, 2009, **131**, 1682.
- 37 B. Huang, C. Si, H. Lee, L. Zhao, J. Wu, B.-L. Gu, and W. Duan, *Appl. Phys. Lett.*, 2010, **97**, 043115.
- 38 A. J. Du, Y. Chen, G. Q. Lu, and S. C. Smith, *Appl. Phys. Lett.*, 2008, **93**, 073102.

- 39 A. J. Du, Y. Chen, Z. H. Zhu, R. Amal, G. Q. Lu, and S. C. Smith, *J. Am. Chem. Soc.*, 2009, **131**, 17354.
- 40 E. J. Kan, X. J. Wu, Z. Y. Li, X. C. Zeng, J. L. Yang, and J. G. Hou, *J. Chem. Phys.*, 2008, **129**, 084712.
- 41 F. W. Zheng, G. Zhou, Z. Liu, J. Wu, W. Duan, B. -L. Gu, and S. B. Zhang, *Phys. Rev. B*, 2008, **78**, 205415.
- 42 B. Huang, C. Si, H. Lee, L. Zhao, J. Wu, B.-L. Gu, and W. Duan, *Appl. Phys. Lett.*, 2010, **97**, 043115.
- 43 Y. W. Son, M. L. Cohen, and S. G. Louie, *Nature (London)*, 2006, **444**, 347.
- 44 E. J. Kan, Z. Y. Li, J. L. Yang, and J. G. Hou, *Appl. Phys. Lett.*, 2007, **91**, 243116.
- 45 A. Du, S. Sanvito and S. C. Smith, *Phys. Rev. Lett.*, 2012, **108**, 197207.
- 46 G. Kresse and J. Hafner, *Phys. Rev. B*, 1993, **47**, 558.
- 47 G. Kresse and J. Hafner, *Comput. Mater. Sci.*, 1996, **6**, 15.
- 48 G. Kresse and J. Furthmüller, *Phys. Rev. B*, 1996, **54**, 11169.
- 49 J. P. Perdew, K. Burke, and M. Ernzerhof, *Phys. Rev. Lett.*, 1996, **77**, 3865.
- 50 P. E. Blöchl, *Phys. Rev. B*, 1994, **50**, 17953.
- 51 G. Kresse and D. Joubert, *Phys. Rev. B*, 1999, **59**, 1758.
- 52 Y. X. Ding, Y. C. Sui, S. C. Tai, *Chem. Eng. Sci.*, 2013, **87**, 194–203.
- 53 M. Zhou, X. W. Li, J. J. Cui, T. T. Liu, T. W. Cai, H. C. Zhang, S. Y. Guan, *Int. J. Electrochem. Sci.*, 2012, **7**, 9984 – 9996.
- 54 Wolfgang Förner and Hassan M. Badawi, *J. Theor. Comput. Chem.*, 2014, **13**, 1350073.
- 55 J. S. Lee, X. Q. Wang, H. M. Luo, and S. Dai, *Adv. Mater.*, 2010, **22**, 1004–1007.
- 56 Y. Z. Xu, Kenichi Yakushijin, and David A. Horne, *J. Org. Chem.*, 1996, **61**, 9569-9571.
- 57 H. C. Zhou, M. W. Zhao, X. M. Zhang, W. Z. Dong, X. P. Wang, H. X. Bu and A. Z. Wang, *J. Phys.: Condens. Mat.*, 2013, **25**, 395501.
- 58 M. W. Zhao and R. Q. Zhang, *Phys. Rev. B*, 2014, **89**, 195427.

- 59 A. Z. Wang, X. M. Zhang, M. W. Zhao, *Nanoscale*, 2014, **6**, 11157-11162.
- 60 C. S. Guo, W. J. Fan, and R. Q. Zhang, *Solid State Commun.*, 2006, **137**, 246–248.
- 61 C. S. Guo, W. J. Fan, and R. Q. Zhang, *Appl. Phys. Lett.*, 2006, **89**, 123103.
- 62 R. Q. Zhang, E. Bertran, and S.-T. Lee, *Diam. Relat. Mater.*, 1998, **7**, 1663.
- 63 Y. G. Yao, F. Ye, X. L. Qi, S. C. Zhang, Z. Fang, *Phys. Rev. B*, 2006, **74**, 165310 ().
- 64 M. Gmitra, S. Kunschuh, C. Ertler, Ambrosch-Draxl, J. Fabian, *Phys. Rev. B*, 2009, **85**, 235431.
- 65 M. W. Zhao, W. Z. Dong, A. Wang, *Sci. Rep.*, 2013, **3**, 3532.
- 66 A. J. Lu, R. Q. Zhang, and S. T. Lee, *Appl. Phys. Lett.*, 2007, **91**, 263107.
- 67 C. Zhang, A. D. Sarkar, R. Q. Zhang, *J. Phys. Chem. C*, 2011, **115**, 23682–23687.

Figure captions:

Fig.1 (a) Schematic representation of graphene-like carbon nitride ($g\text{-C}_9\text{N}_7$). The unit cell is indicated by the yellow shaded area with the two basis vectors of \mathbf{a}_1 and \mathbf{a}_2 . (b) Phonon spectrum of $g\text{-C}_9\text{N}_7$ along the high symmetric points in BZ. Brillouin zone and high symmetric points were also presented. (c) Simulated XRD patterns of three graphitic carbon nitride materials: $g\text{-C}_3\text{N}_4$ (top), $g\text{-C}_4\text{N}_3$ (middle) and $g\text{-C}_9\text{N}_7$ (down).

Fig. 2 (a) The electronic band structures and the total densities of states (TDOS) of the $g\text{-C}_9\text{N}_7$. (b) The spin charge densities of the $g\text{-C}_9\text{N}_7$. (c) The electronic density of states (PDOS) projected onto the C1, C2, N3 and N4 atoms (indexed in Figure 1) of the $g\text{-C}_9\text{N}_7$. (d) The energy bands of the $g\text{-C}_9\text{N}_7$ using advanced exchange functional potentials HSE. The energy at the Fermi level is set to zero.

Fig. 3 The orbital-resolved electron density of states (PDOS) projected onto (a) C1 atom, (b) C2 atom, (c) N3 atom, and (d) N4 atom in the $g\text{-C}_9\text{N}_7$. The energy at the Fermi level is set to zero.

Fig. 4 The initial spin configurations of (a) FM, (b) AFM, and (c) NM in a (2×2) supercell. The relative energies and total magnetic moments of the final states obtained from self-consistent calculations are also presented.

Fig. 5 (a) Evolution of the energy difference between ferromagnetic (FM) and nonmagnetic (NM) states (solid line), and the total magnetic moments of the FM states (dashed line) as a function of tensile strain. (b) The total energies of the system as a function of tensile strain. The sudden drop of energy indicates the fracture of the framework.

Fig. 6 The spin-resolved energy bands of the $g\text{-C}_9\text{N}_7$ at a tensile strain of 2% (a), 3% (b), and 4% (c). The variation of the band gap (Δ) between the two spin channels as a function of tensile strain (d). The energy at the Fermi level is set to zero.

Fig. 7 The wave-functions of the g-C₉N₇ at Γ (a) and K (b) special points. The wave-functions of the g-C₉N₇ at Γ (c) and K (d) special points under a tensile strain of 4%.

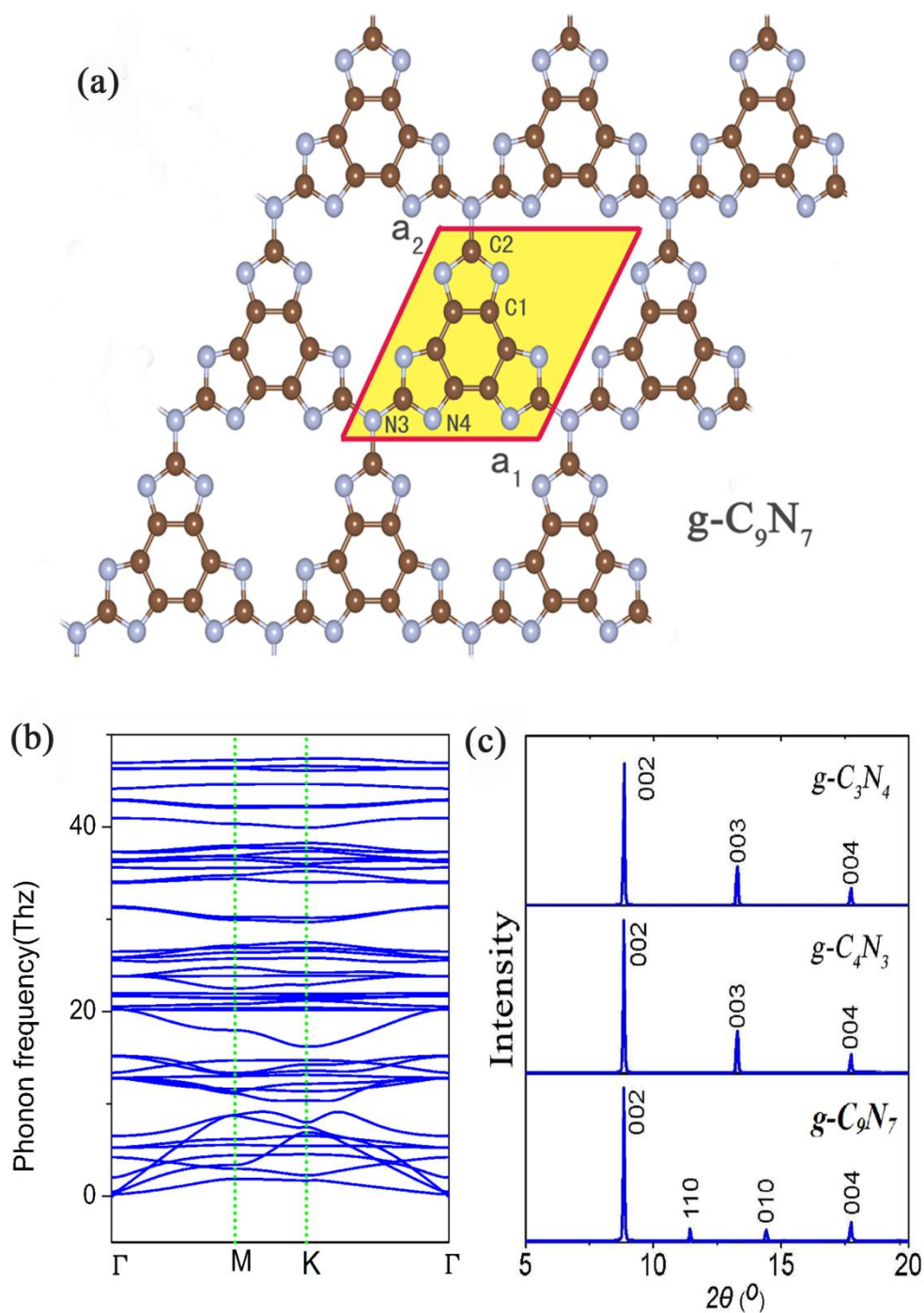


Fig.1 (a) Schematic representation of graphene-like carbon nitride ($g\text{-C}_9\text{N}_7$). The unit cell is indicated by the yellow shaded area with the two basis vectors of \mathbf{a}_1 and \mathbf{a}_2 . (b) Phonon spectrum of $g\text{-C}_9\text{N}_7$ along the high symmetric points in BZ. Brillouin zone and high symmetric points were also presented. (c) Simulated XRD patterns of three graphitic carbon nitride materials: $g\text{-C}_3\text{N}_4$ (top), $g\text{-C}_4\text{N}_3$ (middle) and $g\text{-C}_9\text{N}_7$ (down).

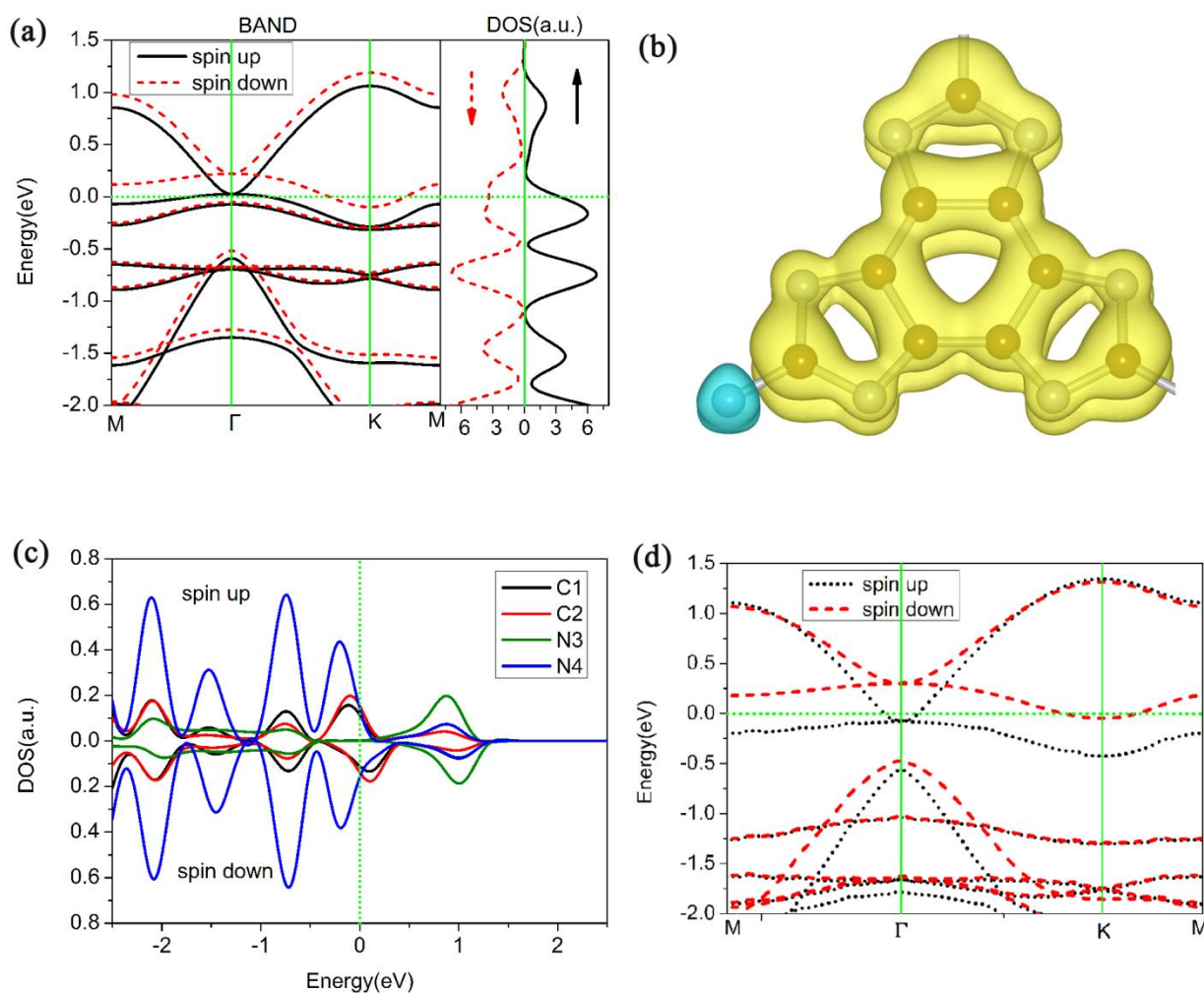


Fig. 2 (a) The electronic band structures and the total densities of states (TDOS) of the $g\text{-C}_9\text{N}_7$. (b) The spin charge densities of the $g\text{-C}_9\text{N}_7$. (c) The electronic density of states (PDOS) projected onto the C1, C2, N3 and N4 atoms (indexed in Figure 1) of the $g\text{-C}_9\text{N}_7$. (d) The energy bands of the $g\text{-C}_9\text{N}_7$ using advanced exchange functional potentials HSE. The energy at the Fermi level is set to zero.

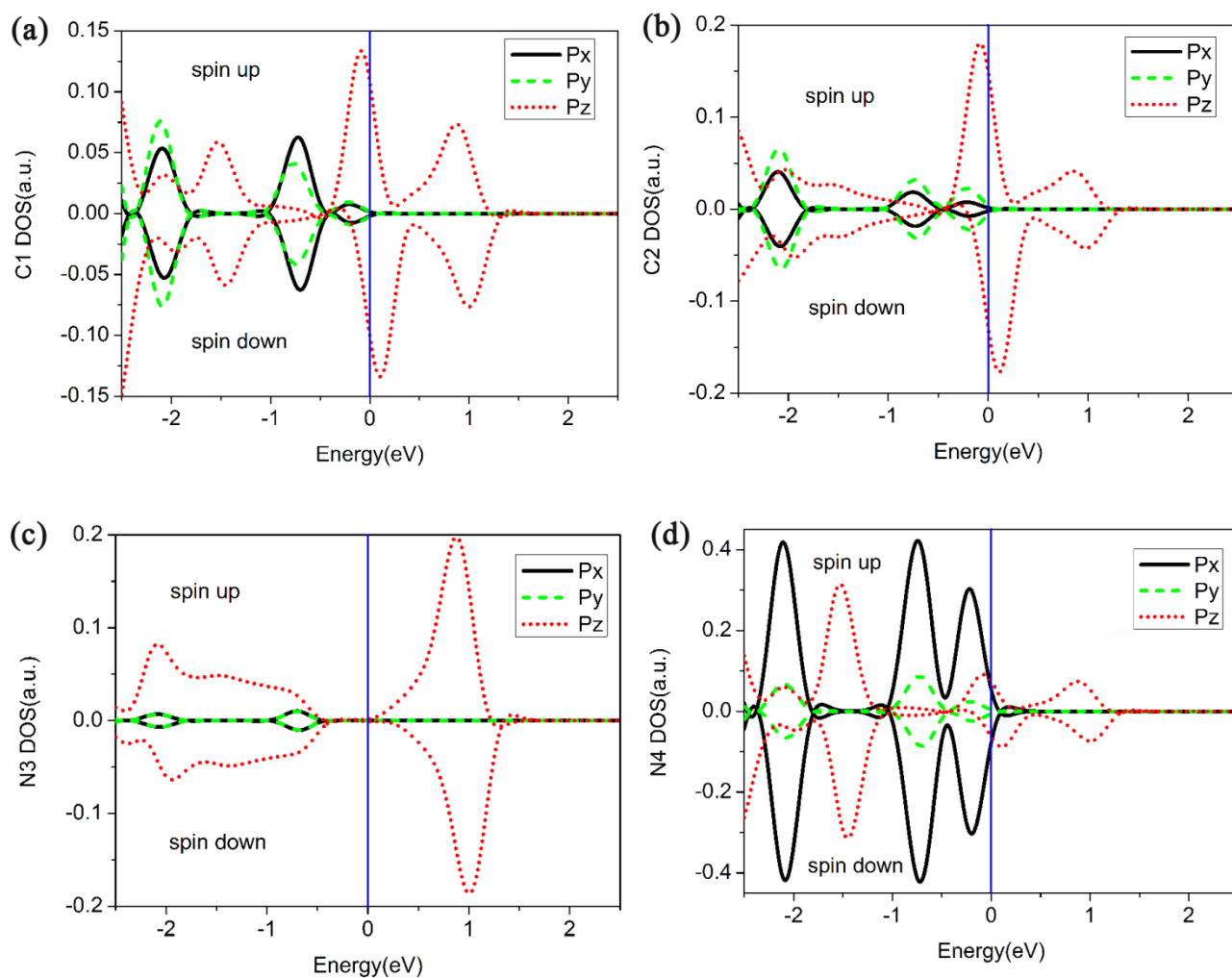


Fig. 3 The orbital-resolved electron density of states (PDOS) projected onto (a) C1 atom, (b) C2 atom, (c) N3 atom, and (d) N4 atom in the g-C₉N₇. The energy at the Fermi level is set to zero.

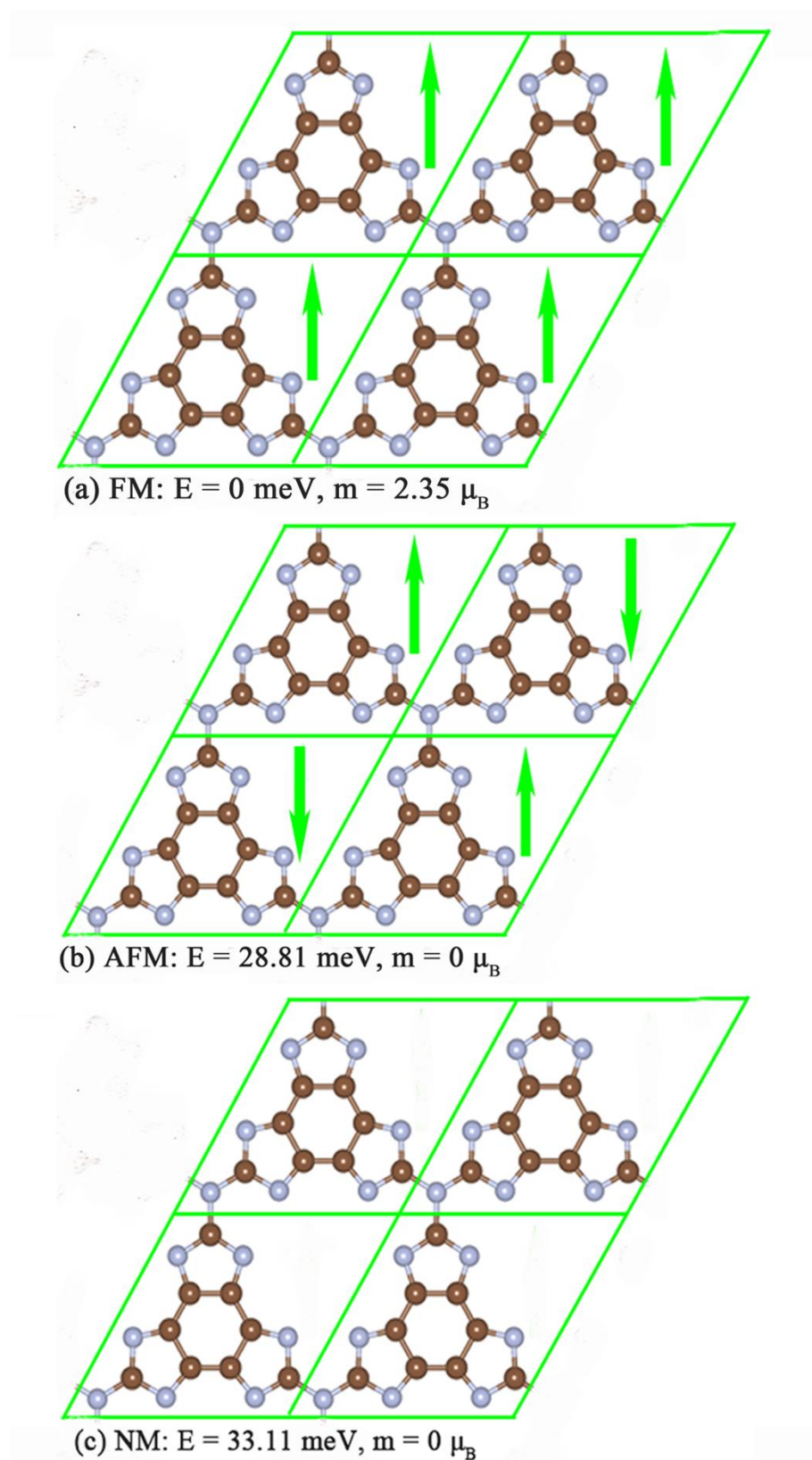


Fig. 4 The initial spin configurations of (a) FM, (b) AFM, and (c) NM in a (2×2) supercell. The relative energies and total magnetic moments of the final states obtained from self-consistent calculations are also presented.

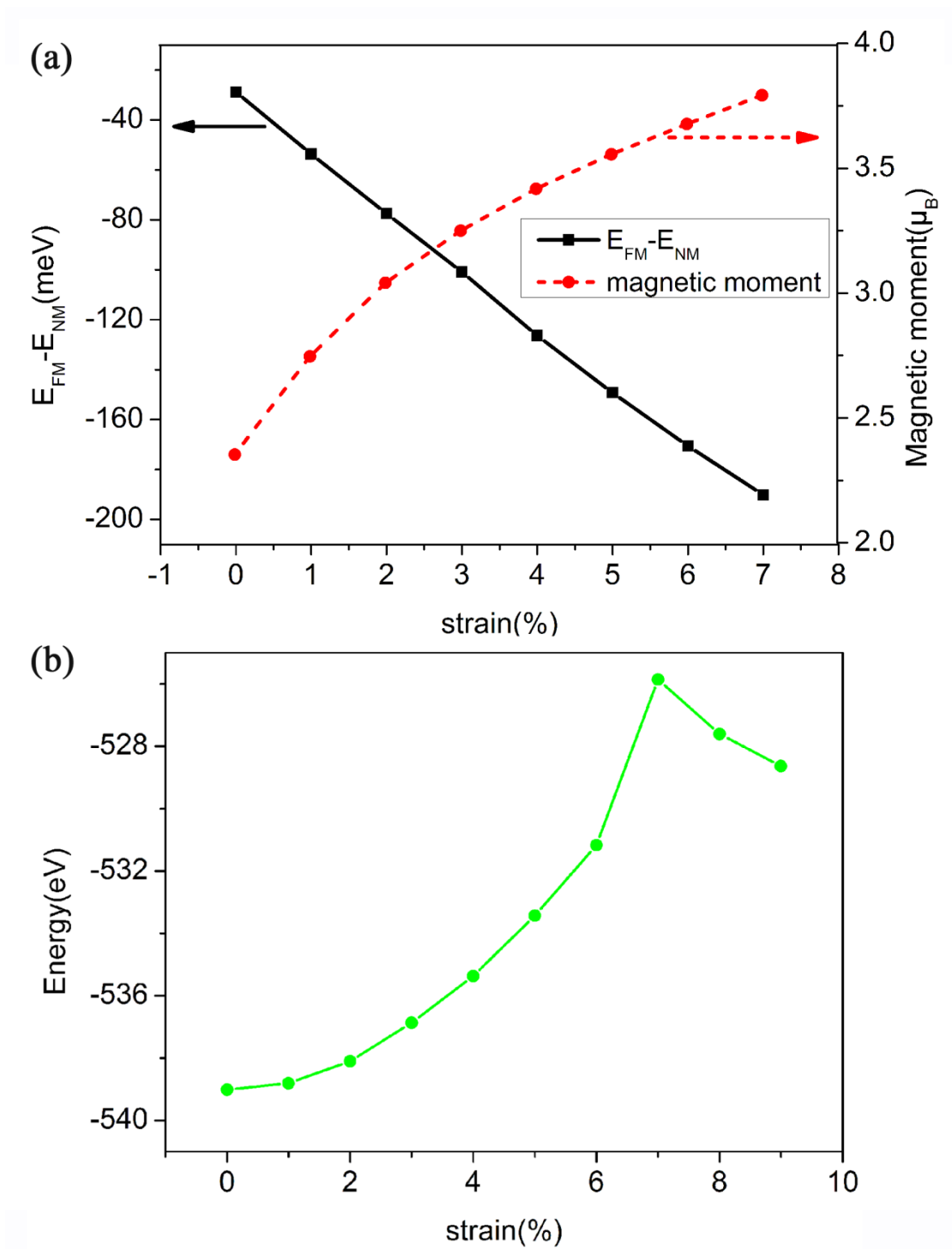


Fig. 5 (a) Evolution of the energy difference between ferromagnetic (FM) and nonmagnetic (NM) states (solid line), and the total magnetic moments of the FM states (dashed line) as a function of tensile strain. (b) The total energies of the system as a function of tensile strain. The sudden drop of energy indicates the fracture of the framework.

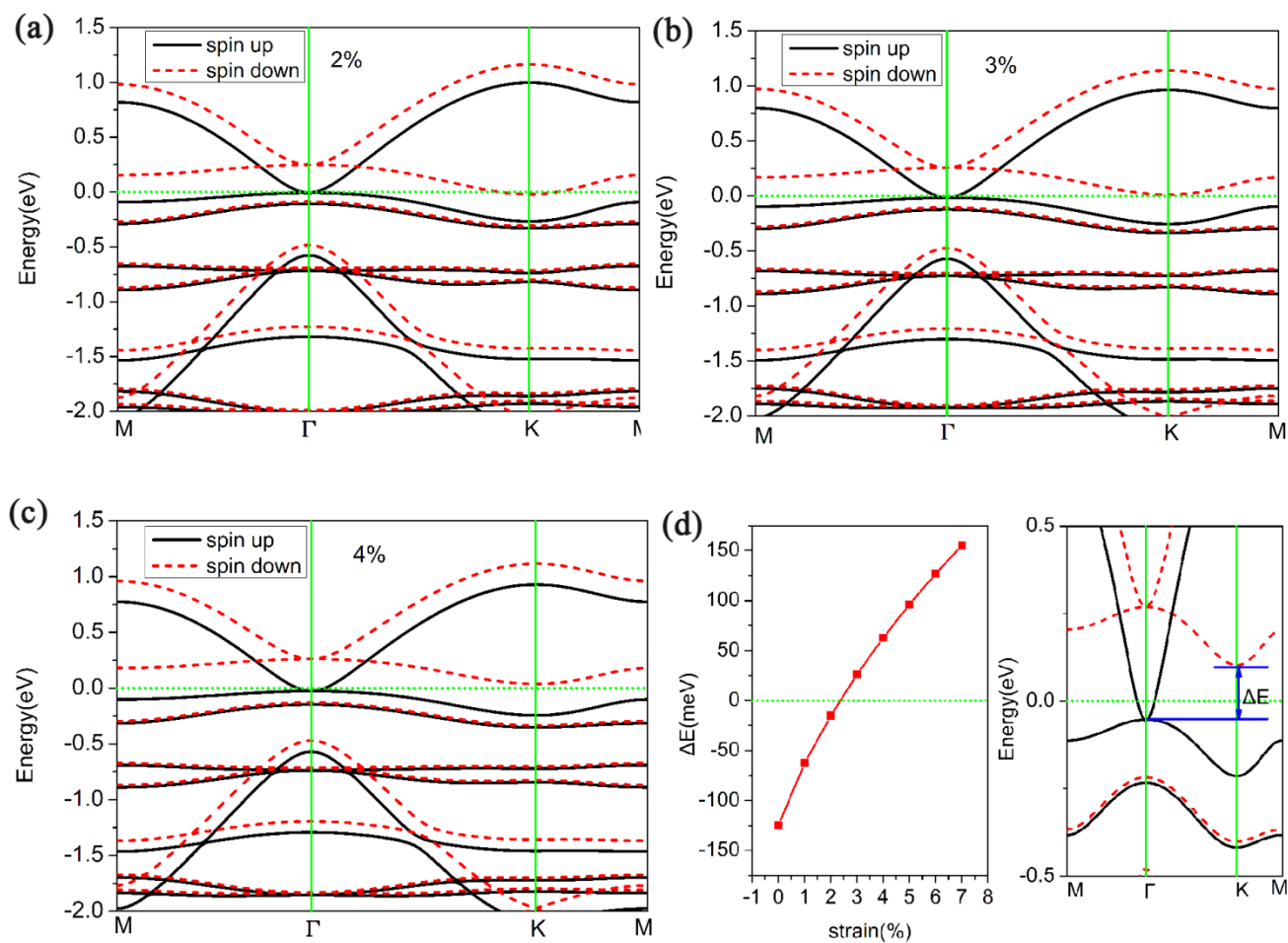


Fig. 6 The spin-resolved energy bands of the $g\text{-C}_9\text{N}_7$ at a tensile strain of 2% (a), 3% (b), and 4% (c). The variation of the band gap (Δ) between the two spin channels as a function of tensile strain (d). The energy at the Fermi level is set to zero.

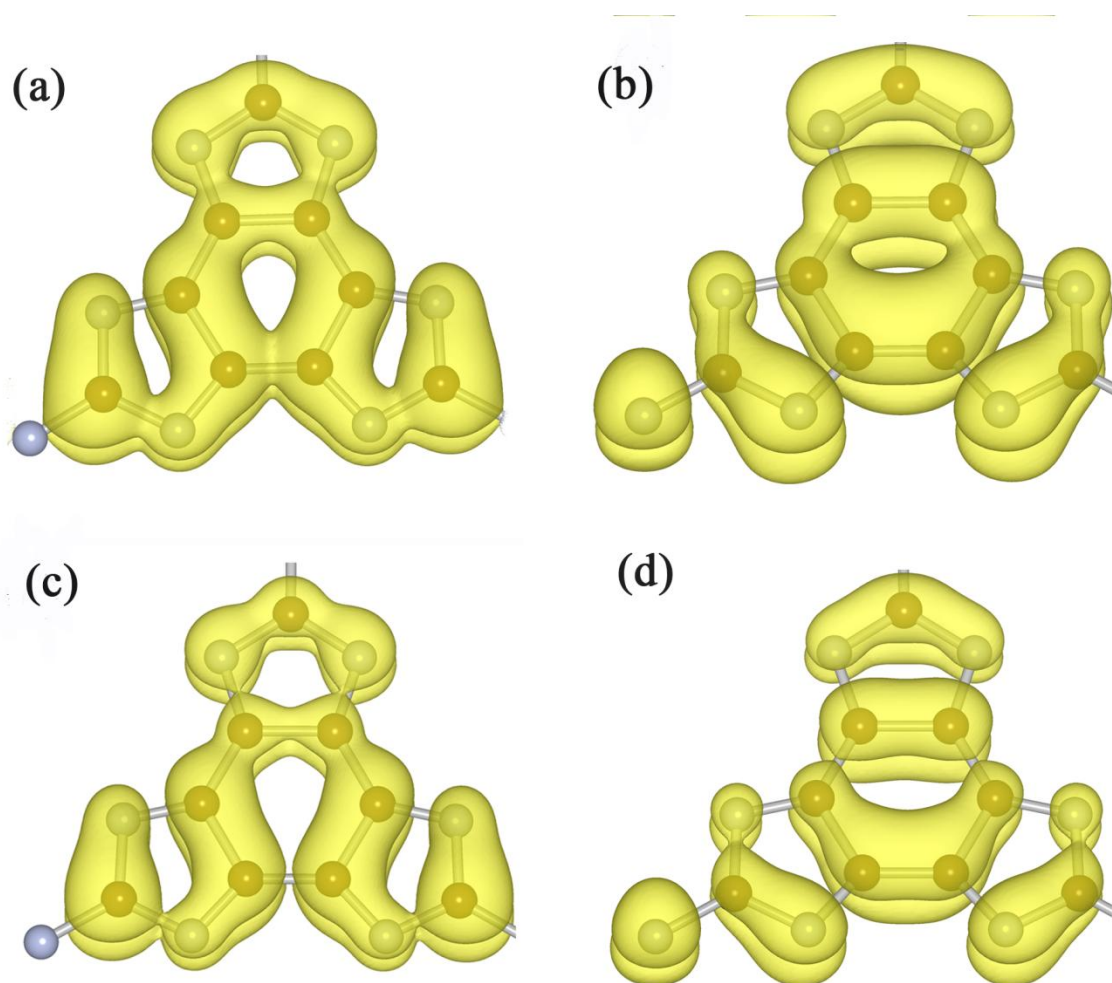


Fig. 7 The wave-functions of the $g\text{-C}_9\text{N}_7$ at Γ (a) and K (b) special points. The wave-functions of the $g\text{-C}_9\text{N}_7$ at Γ (c) and K (d) special points under a tensile strain of 4%.